Mixing and calcite dissolution in heterogeneous coastal aquifers — A numerical 2D study

Kevin De Vriendt[1], Maria Pool[1], Marco Dentz[1]

[1]Institute of Environmental Assessment and Water Research, Spanish National Research Institute

Motivation

To understand the role of heterogeneity and connectivity on mixing and reactivity within a coastal aquifer setting.

Methodology

Connectivity

To evaluate the effect of varying degrees of aquifer connectivity, log-normal multi-Gaussian random permeability fields ($\lambda_x = \lambda_y = 10$m) were transformed as described by [4], resulting in fields characterised by high and low-K pathways.

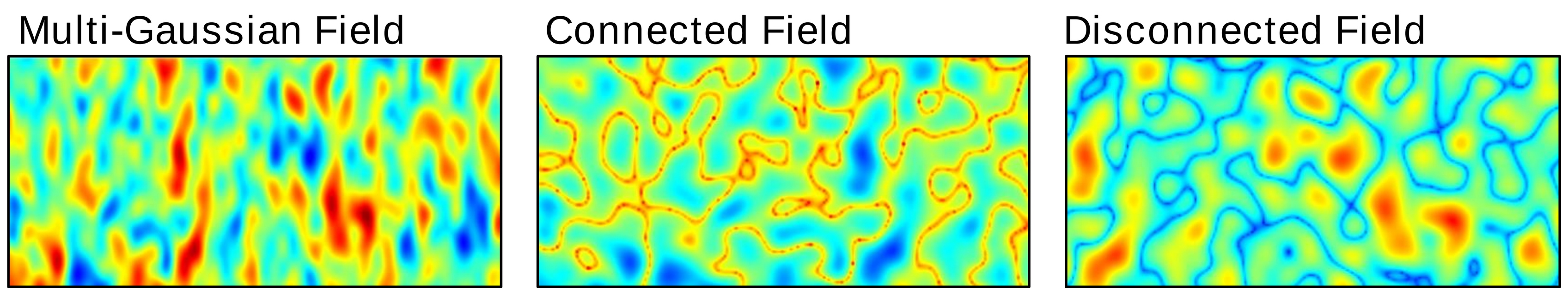

Figure 1: Snapshot of simulated heterogeneous fields

Chemical Reaction

Calcite dissolution is considered using a mixing-ratios based formulation proposed by [3]. The reaction rate is calculated by defining two end-member mixing waters and solving the solution by decoupling solute transport and the chemical speciation problem.

$$r_l(x,z,t) = \underbrace{\varphi_w \rho \frac{\partial^2 c_A}{\partial c^2}}_{\text{Speciation term}} \cdot \underbrace{\nabla c(x,z,t) \cdot \left[\mathbf{D}_h(x,z,t)\nabla c(x,z,t)\right]}_{\chi_L \text{ Scalar Dissipation}} \quad (1)$$

The chemical composition of the mixing waters are defined in the table below.

Table 1: Chemical composition of mixing waters taken from [2]

Solution	pH	Ca	Mg	Na	K	Cl	Log P_{CO_2}
Seawater	7.21	9.64	22.43	496.53	9.28	564.13	-2.01
Freshwater	7.30	1.65	0.00	0.00	0.00	0.00	-2.00

Flow Deformation

Flow deformation inherent to the seawater intrusion problem and resulting from the heterogeneous fields were evaluated to assess its impact on mixing and reaction hotspots. The deformation tensor can be defined as

$$\epsilon_{x,y} = \begin{pmatrix} \frac{\partial vx}{\partial x} & \frac{\partial vx}{\partial y} \\ \frac{\partial vy}{\partial x} & \frac{\partial vy}{\partial y} \end{pmatrix}$$

where the rate of strain, a measure of local stretching deformation is defined by [1]

$$\Theta_\zeta = \underbrace{(2\epsilon_{11})^2}_{\text{normal strain}} + \underbrace{(\epsilon_{21} + \epsilon_{12})^2}_{\text{shear rate}} \quad (2)$$

Local reaction rate and scalar dissipation

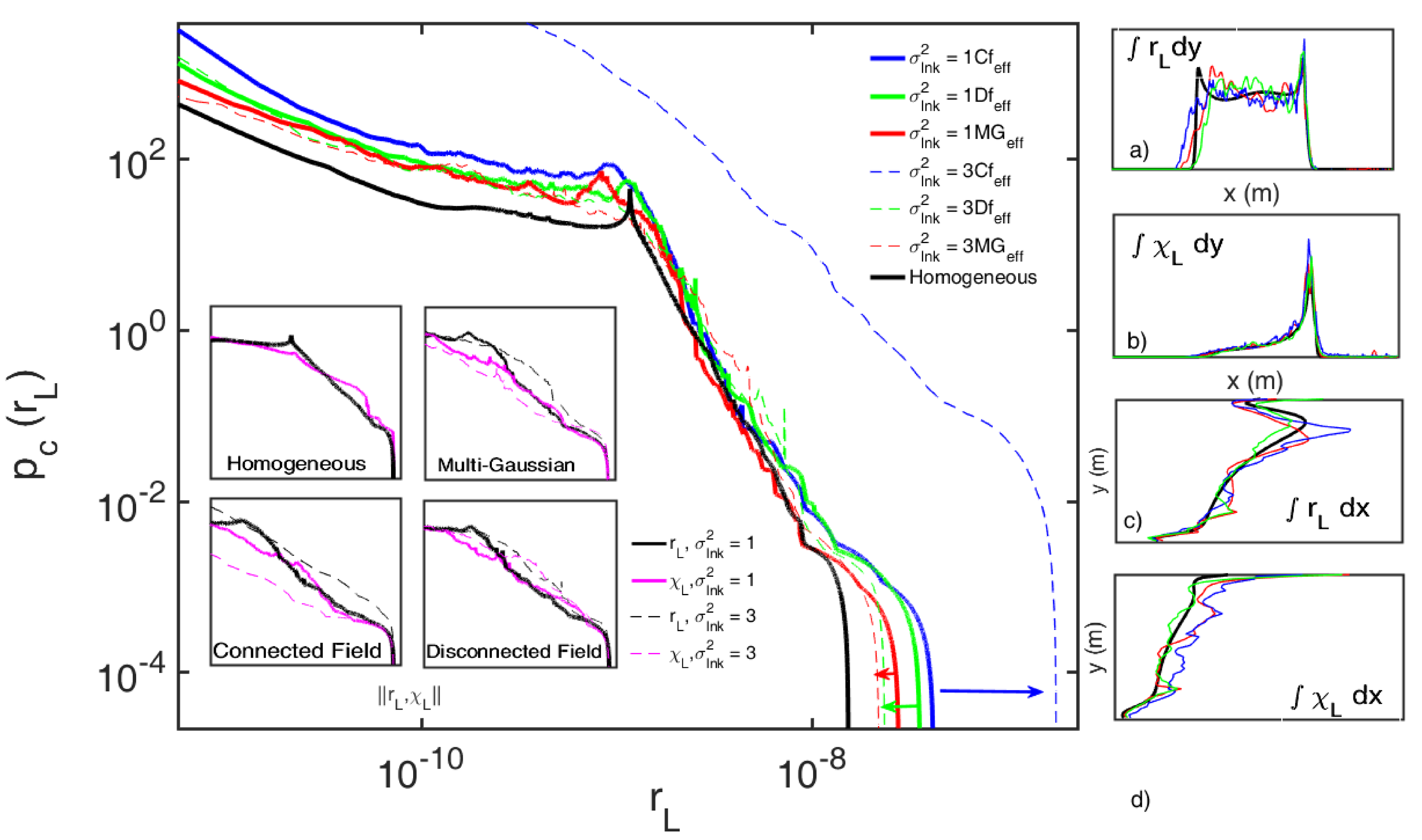

Figure 2: The main figure displays the effective probability density function for local reaction rates. The subset figure show the effective PDF's for the mixing rate and reaction rate where their maxima are normalised in order to assess their local differences. The figures to the left show the vertical and horizontal integration of the reaction and mixing rates.

Acknowledgements

This project has received funding from the European Union's Horizon 2020 research and innovation program under the Marie Sklodowska-Curie Grant Agreement No. 722028.

Numerical Model

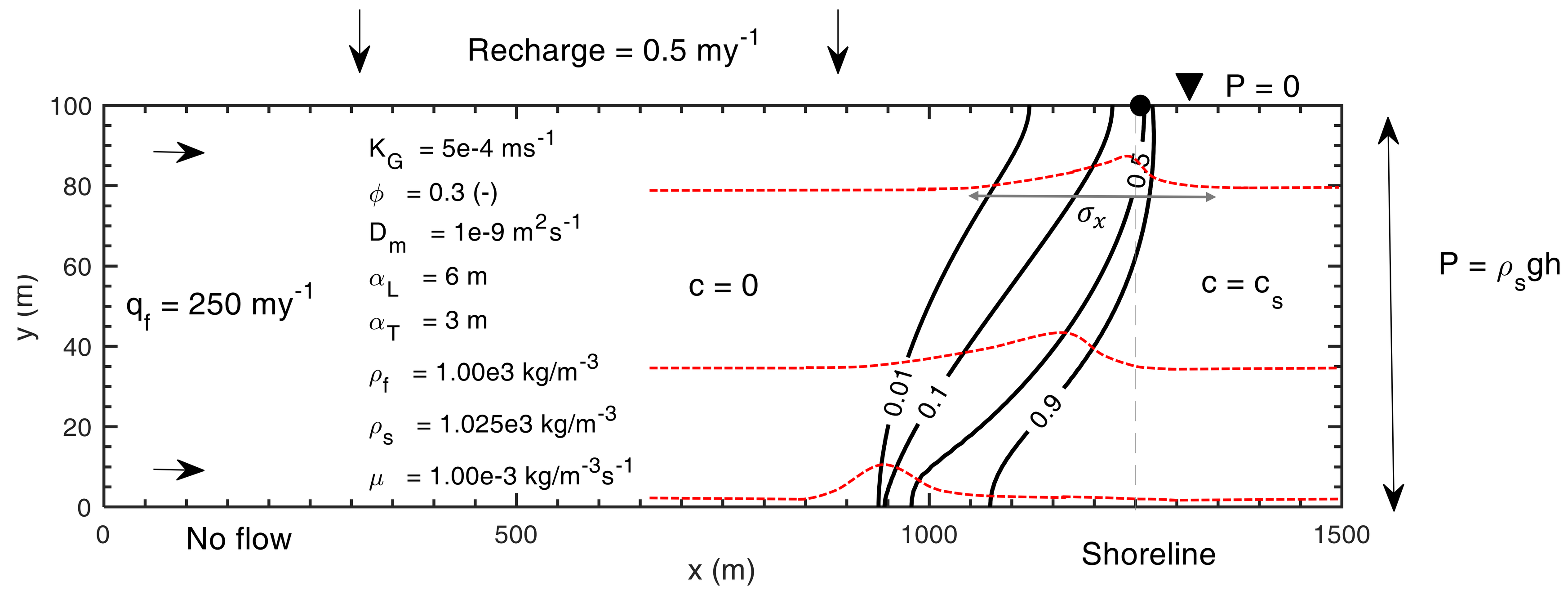

Figure 3: Boundary conditions and input parameters for the numerical model using using COMSOL Multiphysics ®. The red dashed lines represent the vertical and horizontal profiles of the scaled and normalized salt mass fraction distribution

2D numerical results

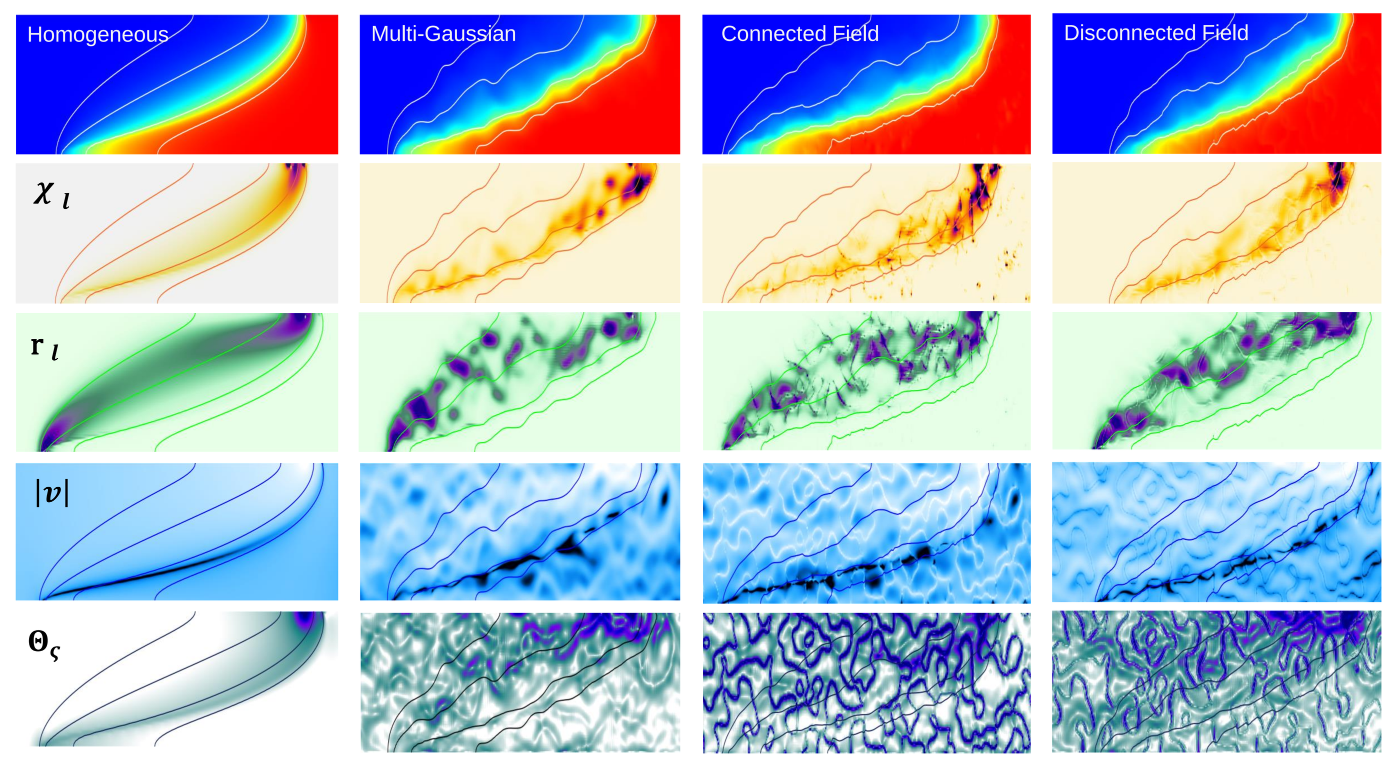

Figure 4: From left to right, we have zoomed in snap-shots for each connectivity field. The top row displays snapshots of the concentration fields which is followed by the mixing rate, the reaction rate, modulus of velocity and the rate of strain. The contour lines denote mixing ratios at 1%,10%,50% and 90%

Global behaviour

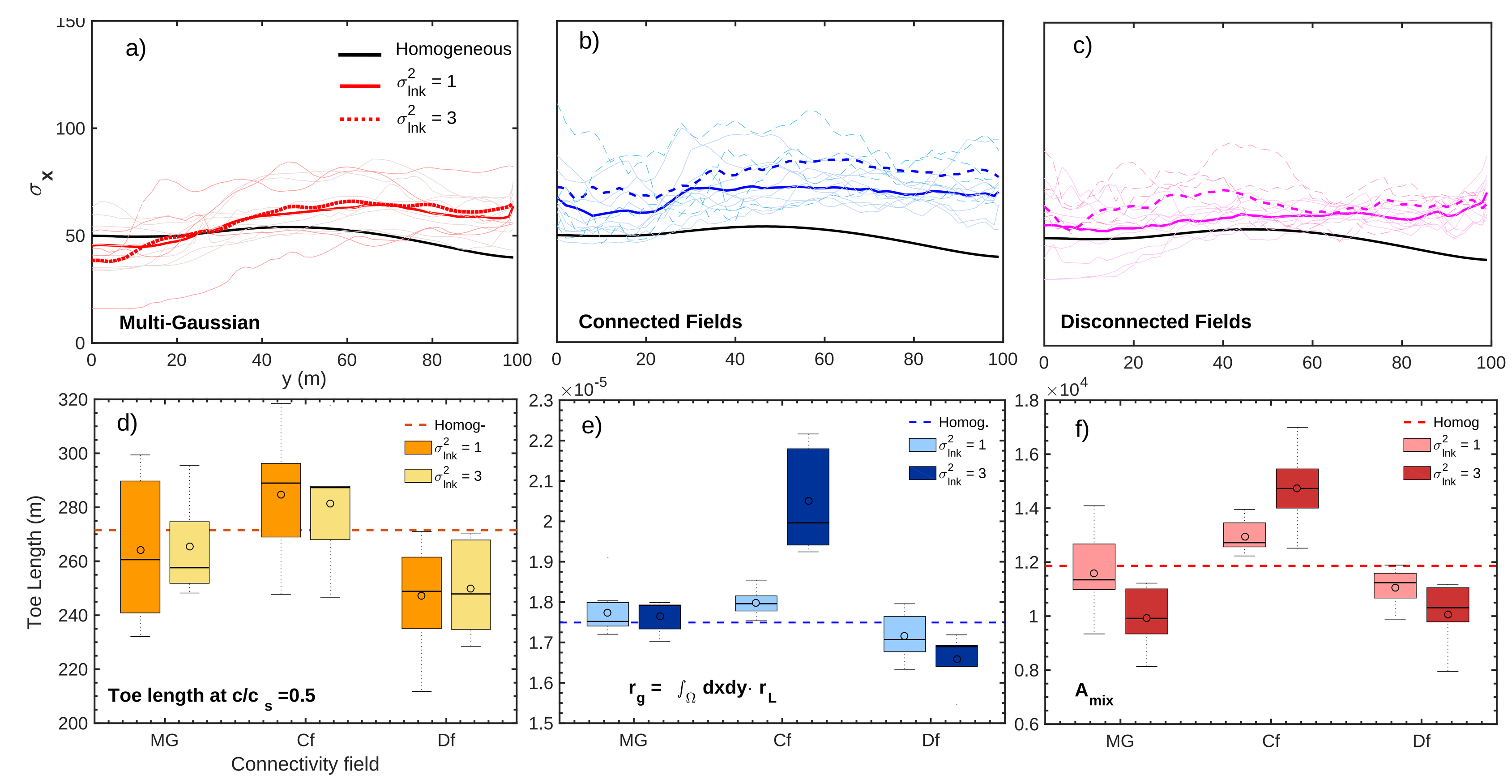

Figure 5: Figures a-c) show the the interface width determined by the second moment of the mixing ratio gradient for all cases of connectivity. Figure d) are the evaluated toe length at a mixing ratio of 50% followed by e) the global reaction rate and f) the mixing area described by 10% and 90% mixing ratios contour lines

Summary

- Despite having fields with near-identical log-normal univariate conductivity distributions, we show the importance of connectivity on local and global reaction rates as well as the extent and width of the mixing zone.
- Connected fields result in the largest observed global and local reaction rates as well as the greatest change in the mixing zone width as demonstrated by the toe length, second spatial moment and the mixing area.
- Large dispersive fluxes near the top of the mixing zone resulting from the convection cell, results in similar local distributions of the reaction rate and scalar dissipation.
- The rate of strain (Θ_ζ) is shown to be a useful proxy in delineating zones of increased mixing. This is predominantly confined to high-K zones or the upper mixing zone.

References

[1] Felipe P J De Barros, Marco Dentz, Jonas Koch, and Wolfgang Nowak. Flow topology and scalar mixing in spatially heterogeneous flow fields. *Geophysical Research Letters*, 39(8):1–5, 2012.

[2] Mohsen Rezaei, Esteban Sanz, Ezat Raeisi, and Carlos Ayora. Reactive transport modeling of calcite dissolution in the fresh-salt water mixing zone. *Journal of Hydrology*, 311:282–298, 2005.

[3] M De Simoni, J Carrera, and M W Saaltink. A mixing ratios-based formulation for multicomponent reactive transport. *Water Resources Research*, 43:1–10, 2007.

[4] Brendan Zinn and Charles F. Harvey. When good statistical models of aquifer heterogeneity go bad: A comparison of flow, dispersion, and mass transfer in connected and multivariate Gaussian hydraulic conductivity fields. *Water Resources Research*, 39(3):1–19, 2003.

kevindevriendt@gmail.com